TITLE

V3 Interneurons Regulate Locomotor Vigor by Recruitment of Spinal Motor Neurons During Fictive Swimming in Larval Zebrafish

ABBREVIATED TITLE

V3 Interneurons Regulate Locomotor Vigor

AUTHOR NAMES AND AFFILIATIONS

Timothy D. Wiggin†, Jacob E. Montgomery†, Amanda J. Brunick, Jack H. Peck, Mark A. Masino

University of Minnesota, Department of Neuroscience, Minneapolis, MN 55455

† Equal contributions.

Corresponding author email: masino@umn.edu

Number of Pages: 47
Number of Figures: 7
Number of Tables: 1
Number of Words for:

Abstract	206
Introduction	521
Discussion	1,310

Conflict of Interest Statement:
The authors declare no competing financial interests.

Acknowledgements:
The authors appreciate the helpful suggestions and feedback from Drs. Ronald Calabrese and Ronald Harris-Warrick. We also thank Kayce Vanpelt for technical support and Marc Tye and the staff of the University of Minnesota Zebrafish Core Facility for animal care. Finally, we thank Drs. Koichi Kawakami and Misha Ahrens for kindly providing *Tg(UAS:GCaMP6s)*^{nk13a} fish.

Financial Support:
This work was supported by National Institutes of Health (http://www.nih.gov/) R01 NS065054 (MAM), R01 NS094176 (MAM), F31 NS083110 (TDW), R25 NS083059 (to Dr. Robert Meisel), Regenerative Medicine Minnesota (JEM), and the Grant-in-Aid of Research, Artistry, and Scholarship (MAM).

ABSTRACT

Survival for vertebrate animals is dependent on the ability to successfully find food, locate a mate, and avoid predation. Each of these behaviors requires fine motor control, which is set by a combination of kinematic properties. For example, the frequency and amplitude (vigor; strength) of motor output combine to determine features of locomotion such as distance traveled and speed. Although there is a good understanding of how different populations of excitatory spinal interneurons establish locomotor frequency, there is not a mechanistic understanding for how locomotor vigor is established. Recent evidence indicates that locomotor vigor is regulated in part by subsets of identified excitatory spinal interneurons (INs), such as the V2a neuronal population in adult zebrafish. Here we provide evidence that the majority of V3 interneurons (V3-INs), which are a developmentally and genetically defined population of ventromedial glutamatergic spinal neurons, are active during fictive swimming. Further, that targeted ablation of V3-INs reduces the proportion of active MNs during fictive swimming, but ablation does not affect the locomotor frequencies produced. These data are consistent with a role of V3-INs in providing excitatory drive to spinal motor neurons during swimming in larval zebrafish, which suggests that locomotor vigor (but not locomotor frequency) may be regulated, in part, by V3-INs.

SIGNIFICANCE STATEMENT

Currently, there is a fundamental lack of knowledge about the cellular and spinal network properties that produce locomotor vigor in vertebrates. Here we show, directly for the first time, that V3 interneurons in zebrafish larvae are active during *in vivo* fictive locomotion, and that targeted ablation of the spinal V3 interneuron population reduces the probability of motoneuron firing during fictive swimming. In contrast to V2a interneurons, ablation of V3 interneurons does not affect locomotor frequency, the fictive neural correlate of speed, which clarifies their role in motor control rather than rhythm generation. Thus, we propose that the V3 interneuron subpopulation is a source of excitation in the vertebrate locomotor neural circuitry that regulates locomotor vigor independently of speed.

INTRODUCTION

Efficient locomotion is set by a combination of kinematic properties, including the frequency and vigor of rhythmic motor output. These properties combine to determine various locomotor features, such as distance traveled and speed (Webb, 1975; Jayne and Lauder, 1995; Donley and Dickson, 2000; Tytell, 2004). Locomotor frequency (e.g. limb or tail-beat rhythmic activity) is a well-studied kinematic variable, which has been shown to increase linearly with speed (Bainbridge, 1958; Hunter and Zweifel, 1971; Webb et al., 1984; Müller and van Leeuwen, 2004). Locomotor vigor is defined as the strength of the motor output and measured as the amplitude of limb displacement in limbed animals during locomotor events (walking, trotting, galloping, hopping (Heglund et al., 1974)) or the amplitude of tail-bend in non-limbed animals (fishes) during undulatory swimming (Wardle et al., 1995; Videler et al., 1999). There is a fundamental understanding of how identified subsets of excitatory spinal interneurons help to establish the frequency of motor output (Crone et al., 2009; Zhong et al., 2011; Ausborn et al., 2012; Eklöf-Ljunggren et al., 2012; Kimura et al., 2013; Ampatzis et al., 2014; Ljunggren et al., 2014; Menelaou et al., 2014; Bellardita and Kiehn, 2015). A critical gap in our knowledge, however, is a mechanistic understanding of the cellular and network properties that regulate locomotor vigor in vertebrate animals.

Across vertebrate species from fish to mammals, the neural circuitry that controls locomotion is located in the ventromedial spinal cord (Grillner and Jessell, 2009; Kiehn, 2011). In vertebrates, developmental gene expression

specifies at least five ventral classes of neuronal progenitor cells. These progenitors give rise to motor neurons (MNs) and four classes of ventral interneurons, referred to as V0 to V3 neurons (Ericson et al., 1997; Pierani et al., 1999). Over the past 10 years, a subset of identified excitatory spinal interneurons (V2a-INs) has been shown to control the speed of locomotion in a variety of vertebrates (Zhong et al., 2011; Ausborn et al., 2012; Ampatzis et al., 2014; Gosgnach et al., 2017). A recent study indicated that V2a-INs in adult zebrafish were involved in both regulating locomotor speed and vigor (Song et al., 2018). To date, however, a subpopulation of spinal interneurons that selectively regulates locomotor vigor has not been identified. In the mammalian spinal cord, a genetically defined subset of pre-motor glutamatergic neurons, called V3 interneurons (V3-INs), contribute to limb coordination, motor burst duration, and muscle spasms, but do not have a clear role in locomotor pattern generation (Chopek et al., 2018; Danner et al., 2019; Lin et al., 2019).

This work shows, directly for the first time, that V3-INs in zebrafish larvae are active during *in vivo* fictive locomotion and, in part, contribute exclusively to locomotor vigor and not to locomotor frequency, which clarifies their role in fine motor control rather than rhythm generation. This is conceptually important because our results support that the V3-IN subpopulation regulates locomotor vigor independently of speed. This difference is a major functional distinction between the V3-INs and V2a-INs since the latter regulate both speed and vigor (Zhong et al., 2011; Ausborn et al., 2012; Ampatzis et al., 2014; Gosgnach et al., 2017; Song et al., 2018).

118

119 **MATERIALS AND METHODS**

120 *Fish Lines and Maintenance*

121 All procedures were approved by the Institutional Animal Care and Use
122 Committee of the University of Minnesota Twin Cities. Wild type (Segrest Farms,
123 Gibsonton, FL) and transgenic adult zebrafish (*Danio rerio*) were maintained in
124 the University of Minnesota Zebrafish Core Facility. The transgenic lines used in
125 these experiments were: *Tg(nkx2.2a:mEGFP)*^{vu17} (Kirby et al., 2006),
126 *Tg(vglut2a:DsRed)*^{nns9} (Miyasaka et al., 2009), *Tg(vglut2a:Gal4ff)*^{nns20} (Satou et
127 al., 2013), *Tg(UAS:GCaMP6s)*^{nk13a} (Muto et al., 2017), *Tg(UAS:Kaede)*^{s1999t}
128 (Scott et al., 2007), and *parga*^{mn2Et} (Balciunas et al., 2004). In-crossed and out-
129 crossed transgenic larvae at 4 – 6 days post fertilization (dpf) were used in these
130 experiments. Larval zebrafish were maintained in petri dishes filled with embryo
131 water (60 µg/ml Instant Ocean® salt mix, Cincinnati, OH) and 0.00005%
132 Methylene Blue in a 28.5°C incubator with a 14:10 light:dark cycle.

133

134 *Kaede Photoconversion*

135 *In vivo* photoconversion of genetically encoded Kaede was performed in
136 *Tg(vglut2a:Gal4ff)*^{nns20}*;Tg(UAS:Kaede)*^{s1999t} larvae using a fixed-objective, upright
137 microscope (Olympus FV-1000, Center Valley, PA). Larvae were anesthetized in
138 zebrafish ringers solution (Wiggin et al., 2012, 2014) with 0.02% Tricaine-S (MS-
139 222; Western Chemical, Ferndale, WA), embedded laterally in a fluorodish
140 (World Precision Instruments, Sarasota, FL) filled with 1.5% low-melting point

141 agarose in zebrafish ringers solution and covered with additional saline
142 containing anesthetic. Photoconversion of Kaede was performed using the
143 bleach function of the FV-1000 to direct a 405 μm laser spot onto a Kaede-
144 expressing cell targeted for conversion (5% laser intensity, 7 s, single pulse). The
145 embedding procedure resulted in small variations in the orientation of the spinal
146 cord such that the larvae were not precisely level and square with respect to the
147 imaging plane. Following confocal stack acquisition, Fiji (Schindelin et al., 2012)
148 was used to rotate the image in order to correct these errors.
149
150 *V3-IN Soma Distribution Analysis*
151 Quantification of the distribution of V3-IN cell bodies was performed using
152 Fiji and custom Matlab code (Mathworks, Natick, MA). Confocal microscopy was
153 used to collect overlapping stacks of images documenting the expression of
154 *Tg(vglut2a:DsRed)*^{nns9} and transmitted light morphology. Images were acquired
155 at high magnification (40X / NA 0.8 objective) and a z-axis resolution of 1.3 μm.
156 The fields of view in each stack overlapped with their neighbors by at least 10%
157 of the width to permit accurate stitching, and included the full width of the spinal
158 cord and dorsal root ganglia (DRG) in the field of view. The collection of stacks
159 was stitched into a single 3-D image of the caudal hindbrain and spinal cord
160 (Preibisch et al., 2009). The Fiji Cell Counter tool was used to identify the
161 coordinates of all V3 neurons in the rostral 2 mm of the larval spinal cord (out of
162 a total length of ~3 mm), the coordinates of the DRG neuron clusters, and the
163 position of the dorsal and ventral edges of the spinal cord. The markers tracing

164 the dorsal and ventral edges of the spinal cord were used to calculate local
165 tangent lines to the dorsal and ventral edges of the spinal cord at the
166 rostrocaudal position of each V3-IN. The equation of a line perpendicular to the
167 ventral tangent and intersecting the V3-IN was calculated, referred to as the "V3
168 plumb line." The rostrocaudal distance of each V3 neuron was calculated as the
169 distance along the ventral surface of the spinal cord between the spinal
170 cord/hindbrain junction (Segment 2/3 boundary) and the V3 plumb line
171 intersection with the ventral surface. The dorsoventral height of the spinal cord at
172 the location of each V3-IN was calculated as the distance between the
173 intersections of the V3 plumb line with the dorsal surface and the ventral surface,
174 respectively. The distance of the V3-IN from the ventral surface of the spinal cord
175 was also measured along the plumb line. The z-axis position of DRG neurons on
176 each side of the spinal cord were used as boundary points of the lateral edges of
177 the spinal cord, and a linear fit to the DRG neurons on each side of the animal
178 was used to calculate the edges of the spinal cord at each rostrocaudal position
179 in the imaging area. The midline slice and spinal cord width were calculated at
180 the rostrocaudal position of each V3-IN, along with the distance from midline of
181 the V3-IN.
182
183 *Whole-mount Immunohistochemistry*
184 Immunohistochemical labeling was conducted using established
185 procedures (Montgomery et al., 2016). Five dpf *parga*^{mn2Et} larvae were sacrificed
186 with 0.2% Tricaine-S and fixed overnight in 4% paraformaldehyde at 4°C. Whole-

187 mount larvae were permeabilized with Proteinase K, post-fixed, and blocked with
188 0.2% BSA, 10% normal donkey serum, 0.5% Triton X-100 in PBS. Goat
189 polyclonal anti-choline acetyltransferase (ChAT; 1:50; AB144P) was added to the
190 blocking solution and incubated overnight at 4°C. Fixed larvae were incubated
191 with Alexa Fluor 633 donkey anti-goat secondary antibody (1:500; A-21082,
192 Thermo Fisher Scientific Inc., Waltham, MA) in secondary blocking solution
193 (0.2% BSA, 1% normal donkey serum, 0.5% Triton X-100 in PBS) for three
194 nights at 4°C.

195 Anti-ChAT labeled *parga*^{mn2Et} larvae were embedded laterally in low
196 melting-point agarose. An Olympus Fluoview FV1000 confocal microscope was
197 used to collect images through a 60x objective centered on body segment 15.
198 Confocal stacks contained the entire dorsoventral extent of the spinal cord and
199 spanned approximately three body segments (285 μm). Images were processed
200 in Fiji (open source image processing package) and labeled cells from a single
201 side of the spinal cord (approximately three hemisegments) were quantified using
202 the Cell Counter plugin. Photoshop CS5 (Adobe Systems, San Jose, CA) was
203 used to adjust brightness and contrast across entire z-projected images.

204

205 *In Vivo Rhod-2 AM Dye Loading of Motor Neurons*

206 For *in vivo* characterization of MNs in *parga*^{mn2Et} larvae, a 0.25% Rhod-2
207 AM (Life Technologies, Grand Island, NY) stock was made by dissolving 50 μg of
208 dye in 20 μL Pluronic F-127:DMSO (1:4; Life Technologies, Grand Island, NY).
209 Next, the skin was removed from the midbody region and a 1:50 dilution of the

210 Rhod-2 AM stock was bath applied to the exposed muscles to permit
211 sequestration of indicator dye by MNs via the peripheral motor axons. Sensory
212 neurons were not strongly loaded by this procedure. Following one-hour
213 incubation, the Rhod-2 AM solution was thoroughly washed-out using zebrafish
214 ringers solution. Confocal images were collected and cells were quantified as
215 described for whole-mount immunohistochemistry (above).
216
217 *Peripheral Nerve Recordings*
218 Peripheral nerve (PN) recordings were performed and analyzed as
219 previously described (Masino and Fetcho, 2005). In brief, the larvae were
220 anesthetized, the skin was carefully removed from the recording region, and
221 larvae were paralyzed with of 0.1 mM α-bungarotoxin (Tocris, Ellisville, MO) to
222 prevent muscle contractions. The anesthetic was removed to allow the larvae to
223 perform fictive behavior, and a suction electrode (tip diameter: 9-15 μm) was
224 placed over the intermyotomal cleft to record MN axons. Fictive motor bursts
225 were identified using custom Matlab code (Wiggin et al., 2012).
226
227 *Calcium Imaging and Analysis*
228 For calcium imaging of V3-INs,
229 *Tg(vglut2a:Gal4ff)*^{nns20}*;Tg(UAS:GCaMP6s)*^{nk13a} zebrafish larvae were used. For
230 calcium imaging of MNs, Calcium Green-1 AM (Life Technologies, Grand Island,
231 NY) dye was loaded into MNs using the protocol for Rhod-2 AM dye loading
232 described above. Larvae were transferred to a fixed-stage Olympus BX51 WI

233 upright microscope with either a 20x / NA 0.5 or a 40x / NA 0.8 water dipping
234 objective lens. A field of view containing *GCaMP6s*-expressing V3-INs in
235 transgenic larvae or Calcium Green-1 AM-loaded MNs in wild type larvae was
236 selected for calcium imaging and a simultaneous peripheral nerve (PN) recording
237 was acquired. Calcium indicator fluorescence was excited with an E-Cite Series
238 120 Q lamp (Excelitas Technologies, Waltham, MA) and acquired at 20 Hz with a
239 Retiga EXi camera and QCapture Pro 6.0 software (QImaging, Surry, BC). Data
240 were acquired during spontaneous fictive swimming in 10-60 s durations for both
241 V3-IN and MN trials. Multiple trials (typically 4) were acquired for each field of
242 view, with at least five min between trials. Movement artifacts during data
243 acquisition were corrected in Fiji by registering frames from all trials to a common
244 reference image (Preibisch et al., 2009). Optical and electrophysiological data
245 acquisition were synchronized by using the sync output of the stimulator to
246 trigger acquisition of the PN recording.

247 For all calcium imaging experiments, raw fluorescence values were
248 determined by drawing a region of interest around each identified V3-IN or MN
249 soma and using the Plot Z-axis Profile command in Fiji. Fluorescence from a
250 region of interest containing background signal was subtracted from raw soma
251 fluorescence measurements to reduce the effect of photobleaching. Baseline
252 fluorescence (F_0) was defined as the mean fluorescence in the first 10 frames of
253 the recording. To calculate $\Delta F/F$, F_0 was subtracted from fluorescence for each
254 frame ($F_{(t)}$), then divided by F_0; $\Delta F/F = (F_{(t)} - F_{(0)}) / F_{(0)}$. A neuron was considered
255 active if $\Delta F/F$ was 10% or greater.

256

257 *Laser Ablation of V3-INs*

258 Acute ablation of the V3-INs was performed using a Micropoint pulsed
259 nitrogen pumped dye laser (Andor Technology, Belfast, Northern Ireland). Light
260 (λ = 435 bm) was delivered via an Olympus BX51 WI microscope using a 60x /
261 NA 1.0 water dipping objective lens. The laser was focused to apply maximal
262 light intensity to the imaging plane of the microscope, the intensity of the laser
263 was calibrated to produce a 4.5 – 5.0 μm hole in a mirror slide (this optimal
264 intensity was determined empirically), and the x-y coordinates of the laser point
265 in the field of view were indicated on a digital display. Three to six dpf
266 *Tg(vglut2a:DsRed)*^{nns9} zebrafish larvae were anesthetized in 0.02% Tricaine in
267 zebrafish ringers solution and embedded laterally in a gel composed of 3%
268 methylcellulose and 0.02% Tricaine in zebrafish ringers saline. A coverslip was
269 placed over the gel and secured at the edges with agarose to stabilize the
270 position of the larvae.

271 Targeted, bilateral laser ablation of DsRed^{+} V3-INs in the ventral spinal
272 cord was performed by positioning the microscope objective such that a neuron
273 was in the x-y position at which the laser was focused. Laser pulses were applied
274 to each V3-IN soma at 33 Hz for 10 s. Laser intensity was empirically determined
275 *a priori* such that >95% of the targeted V3-INs were not present 24 h post-
276 ablation. Following the train of laser pulses, the microscope was repositioned to
277 focus on another identified V3-IN, and the protocol was repeated. Larvae were
278 embedded for approximately 50 min in order to perform bilateral ablation of ~140

279 identified V3-INs between bod segment (S) 5 and S20. To confirm that laser
280 ablation of targeted V3-INs was effective and persistent, the lack of DsRed
281 fluorescence in the lesioned spinal cord of *Tg(vglut2a:DsRed)*^{nns9} larvae was
282 confirmed ~24 hours post-ablation. Sham larvae were treated identically to V3
283 ablation larvae, but the x-y position of the laser was offset by 5 – 20 μm from
284 each V3 cell, producing non-specific damage to neurons other than the V3
285 population.
286
287 *Statistical Analysis*
288 Statistical analysis of data was performed using two-sample *t*-test,
289 ANOVA test, Holm-Sidak post-hoc test, Kolmogorov-Smirnov test, and least-
290 squares linear regression. Statistical tests were carried out using SigmaPlot 12
291 and 14 software (SyStat Software, San Jose, CA), Matlab (Mathworks, Natick,
292 MA), or Microsoft Excel (Microsoft, Seattle, WA). An α level of 0.05 was used to
293 determine statistical significance. Data are reported as means and standard
294 deviation (Mean, SD).
295
296 **RESULTS**
297 *V3-INs are Individually Identifiable in the Larval Zebrafish Spinal Cord*
298 To characterize the functional roles of V3-INs *in vivo*, it was necessary to
299 reliably target the neurons for recording and perturbation. While there are no
300 published transgenic zebrafish lines that specifically label neurons expressing
301 *sim1a* (the zebrafish V3-IN marker), it is possible to infer V3-IN identity from their

302 other characteristics. V3-INs proliferate ventral to the central canal and are
303 glutamatergic (Zhang et al., 2008; Yang et al., 2010). In zebrafish, there is >90%
304 overlap of *vesicular glutamate transporter 2* (*vglut2a*) and *sim1a* expression in
305 the ventral spinal cord at the embryonic stage (1.5 dpf) (Yang et al., 2010).
306 However, it is possible that the embryonic ventral glutamatergic neurons migrate
307 or are replaced by a non-V3 population between 1.5 dpf and the free-swimming
308 larval stage (>3 dpf).

309 To test the hypothesis that the ventral DsRed+ neurons observed in 4 – 6
310 dpf *Tg(vglut2a:DsRed)*^{nns9} larvae are V3-INs, we crossed this line to
311 *Tg(nkx2.2a:mEGFP)*^{vu17}, which marks p3 progenitor neurons (Briscoe et al.,
312 2000; Schäfer et al., 2007) (Fig. 1A). At 4 – 6 dpf, *nkx2.2a:mEGFP* expression
313 was restricted to the region ventral to the central canal (Fig. 1C). The p3 domain
314 of the zebrafish spinal cord also produces Kolmer-Agduhr (KA) neurons (Yang et
315 al., 2010), and likely other neuronal types, so it was expected that there would be
316 more *nkx2.2a:mEGFP*-expressing neurons than *vglut2a:DsRed*-expressing
317 neurons (Fig. 1B). Approximately 94% of *vglut2a:DsRed*-expressing neurons
318 ventral to the central canal also expressed *nkx2.2a:mEGFP* (n = 6 larvae, 162
319 neurons), and were therefore confirmed to be V3-INs (Fig. 1D). There was not a
320 significant difference between the dorsoventral position of the *vglut2a:DsRed*-
321 expressing neurons that co-expressed *nkx2.2a:mEGFP* and those that did not
322 (two-sample t-test; t = 1.6; p = 0.10), so there was not a way to reliably segregate
323 the identified V3-INs, from those that did not express *nkx2.2a:mEGFP*. However,
324 the overwhelming majority of the DsRed^{+} neurons ventral to the central canal

325 were confirmed to be V3-INs. The lack of confirmed transgene overlap in the
326 remaining cells may be due to variegated transgene expression rather than the
327 presence of a non-V3-IN ventral glutamatergic neuronal population. Based on
328 this experiment, we treat the ventral *vglut2a:DsRed*-expressing neurons as the
329 V3-IN population, with the caveat that a small fraction (~6%) may be
330 misidentified.
331
332 *V3-INs are Located in the Ventromedial Spinal Cord and are Distributed Along*
333 *the Rostrocaudal Axis of the Spinal Cord*
334 In mice, the V3-INs migrate following differentiation to form spatially
335 segregated dorsal and ventral populations that have different cellular properties
336 and may be necessary for different behaviors (Borowska et al., 2013). To
337 determine if there are multiple populations of spatially segregated V3-INs in
338 zebrafish larvae, we used confocal microscopy to create 3-D reconstructions of
339 the spinal cords of 4 – 6 dpf *Tg(vglut2a:DsRed)*^{nns9} zebrafish larvae (Fig. 2A-B).
340 The center of each V3-IN soma in the most rostral 2 mm of the spinal cord was
341 tagged, and the distribution of the neurons within the spinal cord was calculated
342 based on the imputed borders of the spinal cord (see *Methods*). Neurons in the
343 far caudal spinal cord were not counted because the dimensions of the spinal
344 cord taper to the extent that it was difficult to determine the location of the central
345 canal and Mauthner axons. All of the neurons (n = 4 larvae; 797 neurons) were
346 located medial of the Mauthner axon (Fig. 2C). V3-IN density was highest in the
347 rostral spinal cord but remained close to 1 cell per 10 μm throughout the cord

348 (Fig. 2D). The V3-IN somas were approximately 5 μm in diameter in the
349 rostrocaudal axis, so a density of ~1 cell per 10 μm thoroughly tiled the ventral
350 spinal cord. The majority of V3-INs were located in the most medial and most
351 ventral 25% of the spinal cord (Figs. 2E & F). There was no parasagittal plane
352 through the medial spinal cord that was unoccupied by V3-INs (Fig. 2E), which
353 suggested that the V3 population may be considered a midline population.
354 However, the density of neurons was not highest at the sagittal midline of the
355 spinal cord, and when cell density was plotted along the population axis of the
356 V3-INs, the point of highest density was adjacent to the spinal cord midline (Fig.
357 2G). Therefore, we propose that distinct left and right populations of V3-INs are
358 present, but that there are not multiple ipsilateral populations of spatially
359 segregated V3-INs in larval zebrafish.
360
361 *V3-INs Project Bilaterally and Have Descending Processes*
362 To characterize the morphologies and putative synaptic connectivity of the
363 V3-INs, we examined the 3-D morphology of individual V3-INs using confocal
364 microscopy (Fig. 3). The density of DsRed fluorescence is too high in the
365 *Tg(vglut2a:DsRed)*^{nns9} transgenic line to accurately trace the processes of a
366 single neuron, so we expressed a photoconvertible protein (Kaede) in
367 *Tg(vglut2a:Gal4)*^{nns20}*;Tg(UAS:Kaede)*^{s1999t} larvae to identify and photoconvert
368 single V3-INs (Fig. 3A-B). Following photoconversion, it was possible to obtain
369 morphological images of the V3-INs (*n* = 5 neurons, 4 larvae; Fig. 3C). Based on
370 this sample of V3 morphologies, it was evident that variation in the projection

371 patterns of the V3-INs was present. For example, the V3-IN imaged in S10 had
372 minimal projection density dorsal or rostral to the cell body, while the V3-IN in
373 S18 predominantly projected rostrally and dorsally (Fig. 3C, Lateral z-Projection).
374 Despite these differences, there were some common features of this sample of
375 V3-IN morphologies. First, the imaged V3-INs possessed bilateral projections,
376 but had a higher density of processes ipsilateral to the cell body (Fig. 3C,
377 Horizontal z-Projection). Second, V3-INs had the greatest density of processes
378 close to the cell body and longer caudal projections than rostral projections (Fig.
379 3C). Third, while the full extent of the descending processes of the S9 and S14
380 neurons is not presented in Fig. 3C, V3-INs had a maximum detectable
381 projection distance shorter than 300 μm. The limited projection length we
382 observed may be due to the Kaede photoconversion method used and should be
383 considered a lower bound on the full extent of the projections of the V3-INs. The
384 projection pattern of the V3-INs appeared to innervate the ventral spinal cord,
385 which is populated by MNs, V2a-INs (Eklöf-Ljunggren et al., 2012; Menelaou and
386 McLean, 2013), other V3-INs, KA neurons, and serotonergic neurons (McLean
387 and Fetcho, 2004; Yang et al., 2010).
388
389 *The Majority of V3-INs are Active During Spontaneous Fictive Swimming*
390 In mice, there is only indirect evidence supporting temporal correlation
391 between V3-IN activity and locomotion (Borowska et al., 2013). To test the
392 hypothesis that activity in the V3-INs is appropriately timed to provide excitatory
393 drive to MNs during locomotion, we monitored the activity of the V3-INs during

394 spontaneous fictive swimming using a genetically-encoded calcium indicator
395 (GCaMP6s; Fig. 4). The activity of V3-INs and fictive motor output during
396 spontaneous swimming was measured via simultaneous calcium imaging and
397 peripheral nerve recording using 4 - 6 dpf
398 *Tg(vglut2a:Gal4ff)*^{nns20}*;Tg(UAS:GCaMP6s)*^{nk13a} larvae (Fig. 4A-B). We found that
399 the majority, 86 of 93 (92%), of V3-INs were active (ΔF/F > 10%) during
400 spontaneous fictive swimming episodes (*n* = 6 larvae, 15 trials). Therefore, this is
401 the first direct evidence that V3-INs are active during fictive locomotion, which
402 supports the participation of V3-INs in producing locomotor activity.
403
404 *Ablation of V3-INs Does Not Affect Episodic or Burst Properties of Spontaneous*
405 *Fictive Swimming*
406 The previous experiments demonstrated that the V3-INs have
407 morphology, neurotransmitter phenotype, and activity consistent with providing
408 excitatory drive to motor neurons but did not demonstrate the function of the V3
409 neurons or their necessity for behavior. To determine whether canonical features
410 of fictive swimming (episode duration, burst (tail-beat) frequency, and burst
411 duration) are modulated by V3-IN activity, we performed laser ablation of a large
412 percentage of the V3-IN population (>95%; ~140 V3-identified somas across
413 body segments 5 to 20; Fig. 5). Three experimental groups were used: 1) The V3
414 ablation group, in which all V3-INs on both sides of the spinal cord between S5
415 and S20 were laser ablated (*n* = 6 larvae; 145 (SD 9.6) neurons per larva).
416 Representative examples of targeted laser ablation efficacy within a restricted

417 region (Fig. 5A-B) and spatial localization (Fig. 5C-D) are shown. 2) The sham
418 ablation group, in which laser pulses were delivered 5 – 20 μm rostral to each
419 identified V3-IN cell body (*n* = 6 larvae; 130 (SD 10.8) sham targets per larva). 3)
420 The unmanipulated control group was not embedded or exposed to laser pulses
421 (*n* = 6 larvae).

422 The day following laser ablation or sham ablation, fictive swimming was
423 measured using PN recordings. Episode duration, burst frequency, and burst
424 duration were not significantly different between unmanipulated, sham and
425 ablation experimental groups during spontaneous swimming (one-way ANOVAs;
426 all $F < 1.3$; all $p > 0.30$; Table 1). These results indicate that the population of
427 spinal V3-INs do not play a significant role in establishing episode duration, burst
428 frequency (a proxy for tail-beat frequency), or burst duration during fictive
429 locomotion in larval zebrafish.

430

431 *Ablation of V3-INs Reduces the Proportion of Active Motor Neurons but Does Not*
432 *Affect Peak Locomotor Frequency During Spontaneous Fictive Swimming*

433 Since the ablation of spinal V3-INs in zebrafish larvae did not affect
434 episode duration, burst frequency, or burst duration (Table 1), we tested the
435 hypothesis that ablation of V3-INs reduces locomotor vigor by decreasing the
436 number of active MNs during spontaneous fictive swimming. In order to ablate
437 V3-INs without also photo-damaging or bleaching motor neurons, we used a two-
438 step neuronal targeting strategy. First, V3-INs were identified and ablated using
439 the *Tg(vglut2a:DsRed)* ^{nns9} transgenic line. Following recovery from laser

440 ablation, motor neurons were loaded with a cell-permanent calcium indicator,
441 Calcium Green-1, AM. To verify that spinal neurons loaded with AM dye (Calcium
442 Green-1 and/or Rhod-2) were MNs, we first confirmed motor neuronal specificity
443 of GFP expression in the *parga*^{mn2Et} enhancer trap line (Balciunas et al., 2004).
444 *Parga*^{mn2Et} larvae immunolabeled for the cholinergic marker choline
445 acetyltransferase (ChAT) revealed that the majority of GFP-expressing neurons
446 co-labeled with ChAT antibodies (*n* = 5; 91.3% (SD2.1); Fig. 6A-A''). A small
447 percentage of dorsally-positioned ChAT+ cells did not colocalize with GFP (4.1%
448 (SD2.8); Fig. 6A-A'', arrowheads); these cells were considered members of a
449 subset of cholinergic spinal interneurons that modulate MN excitability recently
450 identified in zebrafish (Bertuzzi and Ampatzis, 2018). Thus, GFP expression in
451 the *parga*^{mn2Et} enhancer trap line was specific to MNs.
452 Next, to confirm that loading of AM dye was restricted to MNs, the skin
453 was removed from both sides of the body from *parga*^{mn2Et} larvae, in which GFP
454 expression was shown to be limited to MNs (Fig. 6A-A''), and larvae were
455 incubated in zebrafish ringers solution containing Rhod-2 AM dye (*n* = 4; Fig. 6B-
456 B''). Rhod2-AM, which was not used for calcium imaging experiments because it
457 did not produce a strong calcium signal, was used as a proxy for Calcium Green-
458 1 AM since the excitation/emission wavelengths of Calcium Green-1 AM
459 overlapped with, and could not be disambiguated from, GFP expressed in
460 *parga*^{mn2Et} MNs. The majority of GFP-expressing MNs co-labeled with Rhod-2
461 AM (84.3% (SD4.3); Fig. 6B-B''). A small percentage of GFP-negative cells
462 contained Rhod-2 AM (5.4% (SD0.5); Fig. 6B-B'', arrowheads). Taken together,

463 these results confirmed that MNs were selectively labeled with AM dye and,
464 therefore, the cell permeable calcium indicator (Calcium Green-1 AM) could be
465 used to monitor *in vivo* calcium activity in spinal MNs.

466 To examine the effects of V3-IN ablation on the production of fictive
467 locomotor vigor, we determined the proportion of spinal MNs that were active
468 during spontaneous fictive swimming episodes. MN activity in
469 *Tg(vglut2a:DsRed)*^{nns9} larvae was measured using *in vivo* calcium imaging by
470 loading MNs with Calcium Green-1 AM, while peak burst frequency during
471 spontaneous fictive locomotor activity was measured using extracellular PN
472 recordings (Fig. 7A-B). We quantified the proportion of active MNs and peak
473 burst frequencies during spontaneous fictive swimming for Control (50 swim
474 episodes, 4 larvae), Sham Ablated (14 swim episodes, 2 larvae), and V3-IN
475 Ablated (59 swim episodes, 3 larvae) groups. Importantly, there were no
476 differences in the properties of the fictive swimming produced by these larvae,
477 consistent with our prior experiments (Table 1). Neither the distribution of peak
478 burst frequencies (Kolmogorov-Smirnov test < 0.33, $p > 0.14$ for all group
479 comparisons; Fig. 7C), nor the mean peak burst frequencies, were different
480 between Control, Sham, and Ablation Groups (Control = 39.0 Hz (SD8.5); Sham
481 = 36.4 Hz (SD10.7); Ablated = 39.3 Hz (SD8.9); one-way ANOVA, $F = 5.0$, $p =$
482 0.08; Fig. 7D).

483 Assessment of the probability distributions showed that the proportion of
484 active MNs in the Ablated group was significantly reduced compared to both the
485 Control (Kolmogorov-Smirnov test = 0.68, $p < 0.001$) and Sham (Kolmogorov-

486 Smirnov test = 0.54, p = 0.001) groups (Fig. 7E). The proportion of active MNs
487 was not significantly different between the Control and Sham groups
488 (Kolmogorov-Smirnov test = 0.24, p = 0.50; Fig. 7E). Further, V3-IN ablation had
489 a main effect of significantly reducing the proportion of active MNs during
490 spontaneous fictive swimming (Fig. 7F; Control mean = 65.2% (SD16.7); Sham
491 mean = 56.6% (SD24.2); Ablated mean = 41.2% (SD15.6); one-way ANOVA, F =
492 25.3; p < 0.001). Pairwise multiple comparisons (Holm-Sidak; Fig. 7D) revealed
493 significant differences for the proportion of active MNs between both the Control
494 and Ablated groups (t = 7.02, p < 0.001) and the Sham and Ablated groups (t =
495 2.98, p = 0.007), but significant differences were not found between Control and
496 Sham groups (t = 1.54, p = 0.10). These results indicate that V3-INs participate in
497 regulating locomotor vigor by recruitment of spinal MNs but do not regulate burst
498 frequency during spontaneous fictive locomotion.
499
500 **DISCUSSION**
501 The goal of this study was to characterize the potential role of V3-INs in
502 producing locomotor vigor in genetically tractable and optically accessible larval
503 zebrafish. Locomotor vigor, the strength of a locomotor output, is regulated by
504 the recruitment of motor units appropriate to the desired movement: small units
505 for fine behaviors and large units for large movements (Zajac and Faden, 1985;
506 Mendell, 2005). This recruitment pattern of small to large motor units, the so-
507 called size principle, is well established in both mammalian and swimming
508 locomotor systems (Henneman et al., 1965; Gustafsson and Pinter, 1984a,

509 1984b; Cope and Pinter, 1995; McLean et al., 2007; Gabriel et al., 2011).
510 However, investigations into the pre-motor neural mechanisms that contribute to
511 the regulation of locomotor vigor have been difficult in mammals for two primary
512 reasons. First, mammalian spinal locomotor circuits are complicated by the
513 requirements to control and coordinate limbs and joints, rather than simply
514 produce a smooth gradient of motion intensity (Grillner, 2003; Grillner and El
515 Manira, 2020). Second, despite recent progress in tool development, *in vivo*
516 functional manipulations of mammalian spinal locomotor circuits using mini-
517 scopes and fiber-optics are both challenging and somewhat limited in use
518 (Montgomery et al., 2015; Samineni et al., 2017; Canales et al., 2018). Zebrafish
519 larvae provide several advantages over mammalian models for *in vivo* studies:
520 the spinal cords of fish are less complicated than mammals, zebrafish are
521 recognized as a powerful neurogenetic model system, and the translucent nature
522 of zebrafish larvae makes them particularly appropriate for *in vivo* optical
523 methods of investigation. In this study, we found that, unlike the mammalian
524 spinal circuit, V3-INs in the larval zebrafish spinal cord are contained within a
525 single, ventral anatomical domain (Fig. 1-2) and are not necessary to fictive
526 locomotor rhythm (Table 1) (Zhang et al., 2008; Danner et al., 2019). Instead,
527 zebrafish V3-INs are swim-active neurons that are necessary for recruitment of
528 motor neurons during fictive locomotion (Fig. 4, 7), and therefore are most likely
529 necessary for the recruitment of motor units during free-moving locomotion.
530

531 *V3-INs are a population of previously uncharacterized ventral VGlut2a+ neurons*
532 *in larval zebrafish*

533 Here, we report that almost all ventrally-located neurons labeled by the
534 *Tg(vglut2a:DsRed)*^{nns9} and *Tg(vglut2a:Gal4ff)*^{nns20} transgenic lines are V3-IN cells
535 (Figs. 1-5). The V3-INs, a numerous ventromedial population, are distributed
536 across the rostrocaudal axis of the spinal cord (Fig. 2) and project to both sides
537 of the spinal cord, with a richer innervation of the ipsilateral side of the spinal
538 cord (Fig. 3). In this dataset, there are several different V3-IN projection patterns
539 (Fig. 3), but none of these anatomical projection patterns resemble previously
540 characterized ventral neuron cell types, such Kolmer-Agduhr cells (Dale et al.,
541 1987; Bernhardt et al., 1992; Montgomery et al., 2016), ventral serotonergic
542 neurons (Van Raamsdonk et al., 1996; Brustein et al., 2003; McLean and Fetcho,
543 2004; Montgomery et al., 2018), or VeMes (Hale et al., 2001). V3-INs are a
544 morphologically distinct cell type or collection of cell types that have not been
545 characterized through previous experimental approaches.

546 The observed diversity of cell morphology in the V3-IN cell population is
547 similar to the diversity of V3-INs in the mammalian spinal cord (Borowska et al.,
548 2013; Deska-Gauthier et al., 2020). In mammals, the morphology of V3-IN
549 subtypes is correlated with their circuit function (Borowska et al., 2013).
550 However, we have not found evidence for differential recruitment of V3-INs
551 during fictive swimming or functional heterogeneity. It may be that larval
552 zebrafish V3-INs are a primitive class of excitatory spinal INs, as has been
553 previously proposed for *Engrailed1*-expressing inhibitory neurons in zebrafish

554 (Higashijima et al., 2004). However, analysis of cell morphology in zebrafish
555 larvae is complicated by ongoing development in the nervous system and the
556 rostrocaudal developmental gradient (Cole and Ross, 2001). Further experiments
557 are necessary to clarify if these morphologies represent distinct sub-types of V3-
558 INs, developmental stages of a single morphological family, or regional
559 specializations of the V3-INs.
560
561 *Zebrafish V3-INs are active during fictive locomotion*
562 Results indicating that V3-IN activity is directly correlated to fictive
563 locomotor activity in vertebrate preparations has not been convincingly
564 presented. In mice, there is indirect evidence indicating temporal correlation
565 between V3-IN activity and locomotion (Borowska et al., 2013). Through
566 simultaneous optical and electrophysiological recordings, we showed that activity
567 in the majority of V3-INs is correlated to fictive swimming (Fig. 4) and is therefore
568 appropriately timed to provide excitatory drive to MNs during locomotion. Thus,
569 this is the first direct evidence in any vertebrate preparation that V3-INs are
570 active during fictive locomotion, which provides supporting evidence that they
571 may participate in locomotor activity.
572
573 *V3-IN activity is necessary for motor neuron recruitment, but not necessary for*
574 *rhythm generation*
575 Given that V3-INs have been shown to affect both the regularity and
576 coordination of locomotor activity in mice (Zhang et al., 2008), it was surprising

577 that laser ablation of V3-INs in larval zebrafish had no effect on episode duration,
578 mean burst frequency, or burst duration during fictive swimming in larval
579 zebrafish (Table 1). One interpretation of this finding is that despite similarities in
580 gene expression and neurotransmitter profile, pre-motor interneuron function is
581 divergent between axial and tetrapod locomotion. The latter argument has been
582 advanced regarding the V2a interneurons (Dougherty and Kiehn, 2010;
583 Dougherty et al., 2013); the different effects (or lack thereof) of V3-IN ablation in
584 zebrafish and mice may be a second example of the trend. An important
585 difference between the current study and mouse knock-out experiments is the
586 mechanism of ablation. In the current study, V3-INs were ablated acutely, and
587 little time (~24 hours) was given for circuit compensation. In the mouse
588 experiments, on the other hand, V3-INs were ablated or silenced chronically
589 (Zhang et al., 2008; Rabe Bernhardt et al., 2012), leaving opportunity for
590 physiological compensation. Acute silencing experiments using optogenetics
591 could be performed in both species (Arrenberg et al., 2009; Hägglund et al.,
592 2013), and may demonstrate that this difference between species is due to the
593 experimental manipulation rather than the underlying neural circuit.
594 Over the last several years, a subset of identified excitatory spinal
595 interneurons, called V2a interneurons, has been shown to control the speed of
596 locomotion in a variety of vertebrates (Zhong et al., 2011; Ausborn et al., 2012;
597 Ampatzis et al., 2014; Gosgnach et al., 2017). Of particular interest, a recent
598 study also ascribed a role for regulating locomotor vigor to V2a-INs in adult
599 zebrafish (Song et al., 2018). Taken together, these results indicate that V2a-INs

600 are involved in regulating both locomotor speed and vigor. To date, however, a
601 subpopulation of spinal interneurons that selectively regulate locomotor vigor has
602 not been identified. Our work provides evidence that, in zebrafish larvae, V3-INs
603 contribute exclusively to locomotor vigor. Specifically, we show that targeted
604 ablation of V3-INs (Fig. 5) reduces the probability of MN firing during fictive
605 swimming (Fig. 7E-F), but does not affect the range of locomotor frequencies
606 produced (Fig. 7C-D). This suggests that vigor, but not frequency, may be
607 determined, in part, by the proportion of active V3-INs. Thus, we propose that
608 V3-INs are a source of excitation in the vertebrate locomotor neural circuitry that
609 regulate the vigor of locomotor output.
610
611 *Conclusion*
612 The work presented here addressed an important concept regarding
613 motor control; specifically, a fundamental lack of understanding of the cellular
614 properties that produce locomotor vigor in vertebrates. We showed, directly for
615 the first time, that V3-INs in zebrafish larvae are active during *in vivo* fictive
616 locomotion and contribute, at least in part, exclusively to locomotor vigor. Further,
617 targeted ablation of the V3-IN spinal cord population does not affect locomotor
618 frequency (speed), which clarifies their role in fine motor control rather than
619 rhythm generation. Thus, we propose that the V3-IN subpopulation regulates
620 locomotor vigor independently of speed, which is a functional difference between
621 the V3-INs and V2a-INs since the latter regulate both speed and vigor (Zhong et

622 al., 2011; Ausborn et al., 2012; Ampatzis et al., 2014; Gosgnach et al., 2017;

623 Song et al., 2018).

624 REFERENCES

625 Ampatzis K, Song J, Ausborn J, El Manira A (2014) Separate microcircuit
626 modules of distinct v2a interneurons and motoneurons control the speed of
627 locomotion. Neuron 83:934–943 Available at:
628 http://linkinghub.elsevier.com/retrieve/pii/S0896627314006291 [Accessed
629 October 19, 2017].

630 Arrenberg AB, Del Bene F, Baier H (2009) Optical control of zebrafish behavior
631 with halorhodopsin. Proc Natl Acad Sci U S A 106:17968–17973 Available
632 at: http://www.pnas.org/cgi/doi/10.1073/pnas.0906252106 [Accessed
633 October 23, 2017].

634 Ausborn J, Mahmood R, El Manira A (2012) Decoding the rules of recruitment of
635 excitatory interneurons in the adult zebrafish locomotor network. Proc Natl
636 Acad Sci U S A 109:E3631-9 Available at:
637 http://www.pnas.org/cgi/doi/10.1073/pnas.1216256110 [Accessed October
638 19, 2017].

639 Bainbridge R (1958) The Speed of Swimming of Fish as Related to Size and to
640 the Frequency and Amplitude of the Tail Beat. J Exp Biol 35.

641 Balciunas D, Davidson AE, Sivasubbu S, Hermanson SB, Welle Z, Ekker SC
642 (2004) Enhancer trapping in zebrafish using the Sleeping Beauty
643 transposon. BMC Genomics 5.

644 Bellardita C, Kiehn O (2015) Phenotypic Characterization of Speed-Associated
645 Gait Changes in Mice Reveals Modular Organization of Locomotor
646 Networks. Curr Biol 25:1426–1436 Available at:
647 http://www.ncbi.nlm.nih.gov/pubmed/25959968 [Accessed October 23,
648 2017].

649 Bernhardt RR, Patel CK, Wilson SW, Kuwada JY (1992) Axonal trajectories and
650 distribution of GABAergic spinal neurons in wildtype and mutant zebrafish
651 lacking floor plate cells. J Comp Neurol 326:263–272.

652 Bertuzzi M, Ampatzis K (2018) Spinal cholinergic interneurons differentially
653 control motoneuron excitability and alter the locomotor network operational
654 range. Sci Rep 8.

655 Borowska J, Jones CT, Zhang H, Blacklaws J, Goulding M, Zhang Y (2013)
656 Functional subpopulations of V3 interneurons in the mature mouse spinal
657 cord. J Neurosci 33:18553–18565 Available at:
658 http://www.jneurosci.org/cgi/doi/10.1523/JNEUROSCI.2005-13.2013
659 [Accessed October 23, 2017].

660 Briscoe J, Pierani A, Jessell TM, Ericson J (2000) A homeodomain protein code
661 specifies progenitor cell identity and neuronal fate in the ventral neural tube.
662 Cell 101:435–445 Available at:

663 http://www.ncbi.nlm.nih.gov/pubmed/10830170 [Accessed October 22,
664 2017].

665 Brustein E, Chong M, Holmqvist B, Drapeau P (2003) Serotonin Patterns
666 Locomotor Network Activity in the Developing Zebrafish by Modulating
667 Quiescent Periods. J Neurobiol.

668 Canales A, Park S, Kilias A, Anikeeva P (2018) Multifunctional Fibers as Tools
669 for Neuroscience and Neuroengineering. Acc Chem Res 51.

670 Chopek JW, Nascimento F, Beato M, Brownstone RM, Zhang Y (2018) Sub-
671 populations of Spinal V3 Interneurons Form Focal Modules of Layered Pre-
672 motor Microcircuits. Cell Rep 25.

673 Cole LK, Ross LS (2001) Apoptosis in the developing zebrafish embryo. Dev Biol
674 240:123–142.

675 Cope T, Pinter M (1995) The Size Principle: Still Working After All These Years.
676 Physiology 10:280–286.

677 Crone SA, Zhong G, Harris-Warrick R, Sharma K (2009) In mice lacking V2a
678 interneurons, gait depends on speed of locomotion. J Neurosci 29:7098–
679 7109 Available at:
680 http://www.jneurosci.org/cgi/doi/10.1523/JNEUROSCI.1206-09.2009
681 [Accessed October 23, 2017].

682 Dale N, Roberts A, Ottersen OP, Storm-Mathisen J (1987) The morphology and
683 distribution of “Kolmer-Agduhr cells”, a class of cerebrospinal-fluid-
684 contacting neurons revealed in the frog embryo spinal cord by GABA
685 immunocytochemistry. Proc R Soc Lond B Biol Sci.

686 Danner SM, Zhang H, Shevtsova NA, Borowska-Fielding J, Deska-Gauthier D,
687 Rybak IA, Zhang Y (2019) Spinal V3 Interneurons and Left–Right
688 Coordination in Mammalian Locomotion. Front Cell Neurosci.

689 Deska-Gauthier D, Borowska-Fielding J, Jones CT, Zhang Y (2020) The
690 temporal neurogenesis patterning of spinal p3–V3 interneurons into
691 divergent subpopulation assemblies. J Neurosci 40.

692 Donley JM, Dickson KA (2000) Swimming kinematics of juvenile kawakawa tuna
693 (Euthynnus affinis) and chub mackerel (Scomber japonicus). J Exp Biol
694 203:3103–3116 Available at: http://www.ncbi.nlm.nih.gov/pubmed/11003821
695 [Accessed October 23, 2017].

696 Dougherty KJ, Kiehn O (2010) Firing and Cellular Properties of V2a Interneurons
697 in the Rodent Spinal Cord. J Neurosci 30:24–37 Available at:
698 http://www.jneurosci.org/cgi/doi/10.1523/JNEUROSCI.4821-09.2010.

699 Dougherty KJ, Zagoraiou L, Satoh D, Rozani I, Doobar S, Arber S, Jessell TM,
700 Kiehn O (2013) Locomotor Rhythm Generation Linked to the Output of
701 Spinal Shox2 Excitatory Interneurons. Neuron 80:920–933.

Eklöf-Ljunggren E, Haupt S, Ausborn J, Dehnisch I, Uhlén P, Higashijima S, El Manira A (2012) Origin of excitation underlying locomotion in the spinal circuit of zebrafish. Proc Natl Acad Sci U S A 109:5511–5516 Available at: http://www.pnas.org/cgi/doi/10.1073/pnas.1115377109 [Accessed October 19, 2017].

Ericson J, Rashbass P, Schedl A, Brenner-Morton S, Kawakami A, van Heyningen V, Jessell TM, Briscoe J (1997) Pax6 controls progenitor cell identity and neuronal fate in response to graded Shh signaling. Cell 90:169–180 Available at: http://www.ncbi.nlm.nih.gov/pubmed/9230312 [Accessed October 22, 2017].

Gabriel JP, Ausborn J, Ampatzis K, Mahmood R, Eklöf-Ljunggren E, El Manira A (2011) Principles governing recruitment of motoneurons during swimming in zebrafish. Nat Neurosci 14:93–99 Available at: http://www.nature.com/doifinder/10.1038/nn.2704 [Accessed October 19, 2017].

Gosgnach S, Bikoff JB, Dougherty KJ, El Manira A, Lanuza GM, Zhang Y (2017) Delineating the diversity of spinal interneurons in locomotor circuits. J Neurosci 37.

Grillner S (2003) The motor infrastructure: From ion channels to neuronal networks. Nat Rev Neurosci 4.

Grillner S, El Manira A (2020) Current principles of motor control, with special reference to vertebrate locomotion. Physiol Rev 100.

Grillner S, Jessell TM (2009) Measured motion: searching for simplicity in spinal locomotor networks. Curr Opin Neurobiol 19:572–586 Available at: http://www.ncbi.nlm.nih.gov/pubmed/19896834 [Accessed October 20, 2017].

Gustafsson B, Pinter MJ (1984a) An investigation of threshold properties among cat spinal alpha-motoneurones. J Physiol 357:453–483.

Gustafsson B, Pinter MJ (1984b) Relations among passive electrical properties of lumbar alpha-motoneurones of the cat. J Physiol 356:401–431.

Hägglund M, Dougherty KJ, Borgius L, Itohara S, Iwasato T, Kiehn O (2013) Optogenetic dissection reveals multiple rhythmogenic modules underlying locomotion. Proc Natl Acad Sci U S A 110:11589–11594.

Hale ME, Ritter DA, Fetcho JR (2001) A confocal study of spinal interneurons in living larval zebrafish. J Comp Neurol 437:1–16 Available at: http://www.ncbi.nlm.nih.gov/pubmed/11477593 [Accessed October 19, 2017].

Heglund NC, Taylor CR, Mcmahon TA (1974) Scaling stride frequency and gait to animal size: Mice to horses. Science (80-) 186.

741 HENNEMAN E, SOMJEN G, CARPENTER DO (1965) Functional Significance of
742 Cell Size in Spinal Motoneurons. J Neurophysiol 28:560–580.

743 Higashijima S, Masino MA, Mandel G, Fetcho JR (2004) Engrailed-1 expression
744 marks a primitive class of inhibitory spinal interneuron. J Neurosci 24:5827–
745 5839 Available at: http://www.ncbi.nlm.nih.gov/pubmed/15215305 [Accessed
746 October 19, 2017].

747 Hunter JR, Zweifel JR (1971) Swimming speed, tail beat frequency, tail beat
748 amplitude, and size in jack makerel, Trachurus symmetricus, and other
749 fishes. Fish Bull 69:253–267 Available at:
750 http://swfsc.noaa.gov/publications/CR/1971/7114.PDF [Accessed October
751 23, 2017].

752 Jayne BC, Lauder GV (1995) Speed effects on midline kinematics during steady
753 undulatory swimming of largemouth bass, Micropterus salmoides. J Exp Biol
754 198:585–602 Available at: http://www.ncbi.nlm.nih.gov/pubmed/9318295
755 [Accessed October 23, 2017].

756 Kiehn O (2011) Development and functional organization of spinal locomotor
757 circuits. Curr Opin Neurobiol 21:100–109 Available at:
758 http://www.ncbi.nlm.nih.gov/pubmed/20889331 [Accessed October 20,
759 2017].

760 Kimura Y, Satou C, Fujioka S, Shoji W, Umeda K, Ishizuka T, Yawo H,
761 Higashijima S (2013) Hindbrain V2a Neurons in the Excitation of Spinal
762 Locomotor Circuits during Zebrafish Swimming. Curr Biol 23:843–849
763 Available at: http://www.ncbi.nlm.nih.gov/pubmed/23623549 [Accessed
764 October 20, 2017].

765 Kirby BB, Takada N, Latimer AJ, Shin J, Carney TJ, Kelsh RN, Appel B (2006) In
766 vivo time-lapse imaging shows dynamic oligodendrocyte progenitor behavior
767 during zebrafish development. Nat Neurosci.

768 Lin S, Li Y, Lucas-Osma AM, Hari K, Stephens MJ, Singla R, Heckman CJ,
769 Zhang Y, Fouad K, Fenrich KK, Bennett DJ (2019) Locomotor-related V3
770 interneurons initiate and coordinate muscles spasms after spinal cord injury.
771 J Neurophysiol.

772 Ljunggren EE, Haupt S, Ausborn J, Ampatzis K, El Manira A (2014) Optogenetic
773 activation of excitatory premotor interneurons is sufficient to generate
774 coordinated locomotor activity in larval zebrafish. J Neurosci 34:134–139
775 Available at: http://www.jneurosci.org/cgi/doi/10.1523/JNEUROSCI.4087-
776 13.2014 [Accessed October 19, 2017].

777 Masino MA, Fetcho JR (2005) Fictive swimming motor patterns in wild type and
778 mutant larval zebrafish. J Neurophysiol 93:3177–3188 Available at:
779 http://www.ncbi.nlm.nih.gov/pubmed/15673549 [Accessed October 19,
780 2017].

McLean DL, Fan J, Higashijima S, Hale ME, Fetcho JR (2007) A topographic map of recruitment in spinal cord. Nature 446:71–75 Available at: http://www.ncbi.nlm.nih.gov/pubmed/17330042 [Accessed October 19, 2017].

McLean DL, Fetcho JR (2004) Ontogeny and innervation patterns of dopaminergic, noradrenergic, and serotonergic neurons in larval zebrafish. J Comp Neurol 480:38–56 Available at: http://www.ncbi.nlm.nih.gov/pubmed/15515022 [Accessed October 19, 2017].

Mendell LM (2005) The size principle: A rule describing the recruitment of motoneurons. J Neurophysiol 93:3024–3026.

Menelaou E, McLean DL (2013) Speed control: spinal interneurons with crossed purposes. Curr Biol 23:R716-8 Available at: http://linkinghub.elsevier.com/retrieve/pii/S0960982213009251 [Accessed October 19, 2017].

Menelaou E, VanDunk C, McLean DL (2014) Differences in the morphology of spinal V2a neurons reflect their recruitment order during swimming in larval zebrafish. J Comp Neurol 522:1232–1248 Available at: http://doi.wiley.com/10.1002/cne.23465 [Accessed October 19, 2017].

Miyasaka N, Morimoto K, Tsubokawa T, Higashijima S, Okamoto H, Yoshihara Y (2009) From the olfactory bulb to higher brain centers: genetic visualization of secondary olfactory pathways in zebrafish. J Neurosci 29:4756–4767 Available at: http://www.jneurosci.org/cgi/doi/10.1523/JNEUROSCI.0118-09.2009 [Accessed October 20, 2017].

Montgomery JE, Wahlstrom-Helgren S, Wiggin TD, Corwin BM, Lillesaar C, Masino MA (2018) Intraspinal serotonergic signaling suppresses locomotor activity in larval zebrafish. Dev Neurobiol.

Montgomery JE, Wiggin TD, Rivera-Perez LM, Lillesaar C, Masino MA (2016) Intraspinal serotonergic neurons consist of two, temporally distinct populations in developing zebrafish. Dev Neurobiol 76:673–687 Available at: http://doi.wiley.com/10.1002/dneu.22352 [Accessed October 19, 2017].

Montgomery KL, Yeh AJ, Ho JS, Tsao V, Iyer SM, Grosenick L, Ferenczi EA, Tanabe Y, Deisseroth K, Delp SL, Poon ASY (2015) Wirelessly powered, fully internal optogenetics for brain, spinal and peripheral circuits in mice. Nat Methods 12.

Müller UK, van Leeuwen JL (2004) Swimming of larval zebrafish: ontogeny of body waves and implications for locomotory development. J Exp Biol 207:853–868 Available at: http://www.ncbi.nlm.nih.gov/pubmed/14747416 [Accessed October 22, 2017].

Muto A, Lal P, Ailani D, Abe G, Itoh M, Kawakami K (2017) Activation of the

821 hypothalamic feeding centre upon visual prey detection. Nat Commun.

822 Pierani A, Brenner-Morton S, Chiang C, Jessell TM (1999) A sonic hedgehog-
823 independent, retinoid-activated pathway of neurogenesis in the ventral spinal
824 cord. Cell 97:903–915 Available at:
825 http://www.ncbi.nlm.nih.gov/pubmed/10399918 [Accessed October 22,
826 2017].

827 Preibisch S, Saalfeld S, Tomancak P (2009) Globally optimal stitching of tiled 3D
828 microscopic image acquisitions. Bioinformatics.

829 Rabe Bernhardt N, Memic F, Gezelius H, Thiebes A-L, Vallstedt A, Kullander K
830 (2012) DCC mediated axon guidance of spinal interneurons is essential for
831 normal locomotor central pattern generator function. Dev Biol 366:279–289
832 Available at: http://linkinghub.elsevier.com/retrieve/pii/S0012160612001807
833 [Accessed October 20, 2017].

834 Samineni VK et al. (2017) Fully implantable, battery-free wireless optoelectronic
835 devices for spinal optogenetics. Pain 158.

836 Satou C, Kimura Y, Hirata H, Suster ML, Kawakami K, Higashijima S -i. (2013)
837 Transgenic tools to characterize neuronal properties of discrete populations
838 of zebrafish neurons. Development 140:3927–3931 Available at:
839 http://www.ncbi.nlm.nih.gov/pubmed/23946442 [Accessed October 20,
840 2017].

841 Schäfer M, Kinzel D, Winkler C (2007) Discontinuous organization and
842 specification of the lateral floor plate in zebrafish. Dev Biol 301:117–129
843 Available at: http://linkinghub.elsevier.com/retrieve/pii/S001216060601219X
844 [Accessed October 25, 2017].

845 Schindelin J, Arg I, Arganda-Carreras I, a-Carreras, Frise E, Kaynig V, Longair
846 M, Pietzsch T, Preibisch S, Rueden C, Saalfeld S, Schmid B, Tinevez J-Y,
847 White D, Hartenstein V, Eliceiri K, Tomancak P, Cardona A (2012) Fiji: an
848 open-source platform for biological-image analysis. Nat Methods 9.

849 Scott EK, Mason L, Arrenberg AB, Ziv L, Gosse NJ, Xiao T, Chi NC, Asakawa K,
850 Kawakami K, Baier H (2007) Targeting neural circuitry in zebrafish using
851 GAL4 enhancer trapping. Nat Methods.

852 Song J, Dahlberg E, El Manira A (2018) V2a interneuron diversity tailors spinal
853 circuit organization to control the vigor of locomotor movements. Nat
854 Commun.

855 Tytell ED (2004) The hydrodynamics of eel swimming II. Effect of swimming
856 speed. J Exp Biol 207:3265–3279 Available at:
857 http://www.ncbi.nlm.nih.gov/pubmed/15326203 [Accessed October 23,
858 2017].

859 Van Raamsdonk W, Bosch TJ, Smit-Onel MJ, Maslam S (1996) Organisation of

the zebrafish spinal cord: distribution of motoneuron dendrites and 5-HT containing cells. Eur J Morphol.

Videler JJ, Müller UK, Stamhuis EJ (1999) Aquatic vertebrate locomotion: Wakes from body waves. J Exp Biol 202.

Wardle, Videler, Altringham (1995) Tuning in to fish swimming waves: body form, swimming mode and muscle function. J Exp Biol 198.

Webb PW (1975) Hydrodynamics and energetics of fish propulsion. Bull Fish Res Board Canada 190:1–159 Available at: http://www.dfo-mpo.gc.ca/library/1486.pdf [Accessed October 23, 2017].

Webb PW, KOSTECKI PT, STEVENS ED (1984) The Effect of Size and Swimming Speed on Locomotor Kinematics of Rainbow Trout. J Exp Biol 109.

Wiggin TD, Anderson TM, Eian J, Peck JH, Masino MA (2012) Episodic swimming in the larval zebrafish is generated by a spatially distributed spinal network with modular functional organization. J Neurophysiol 108:925–934 Available at: http://jn.physiology.org/cgi/doi/10.1152/jn.00233.2012 [Accessed October 19, 2017].

Wiggin TD, Peck JH, Masino MA (2014) Coordination of fictive motor activity in the larval zebrafish is generated by non-segmental mechanisms. Bene F Del, ed. PLoS One 9:e109117 Available at: http://dx.plos.org/10.1371/journal.pone.0109117 [Accessed October 19, 2017].

Yang L, Rastegar S, Strähle U (2010) Regulatory interactions specifying Kolmer-Agduhr interneurons. Development 137:2713–2722 Available at: http://dev.biologists.org/cgi/doi/10.1242/dev.048470 [Accessed October 20, 2017].

Zajac FE, Faden JS (1985) Relationship among recruitment order, axonal conduction velocity, and muscle-unit properties of type-identified motor units in cat plantaris muscle. J Neurophysiol 53:1303–1322.

Zhang Y, Narayan S, Geiman E, Lanuza GM, Velasquez T, Shanks B, Akay T, Dyck J, Pearson K, Gosgnach S, Fan CM, Goulding M (2008) V3 Spinal Neurons Establish a Robust and Balanced Locomotor Rhythm during Walking. Neuron 60:84–96 Available at: http://linkinghub.elsevier.com/retrieve/pii/S0896627308008064 [Accessed October 20, 2017].

Zhong G, Sharma K, Harris-Warrick RM (2011) Frequency-dependent recruitment of V2a interneurons during fictive locomotion in the mouse spinal cord. Nat Commun 2:274 Available at: http://www.nature.com/doifinder/10.1038/ncomms1276 [Accessed October 19, 2017].

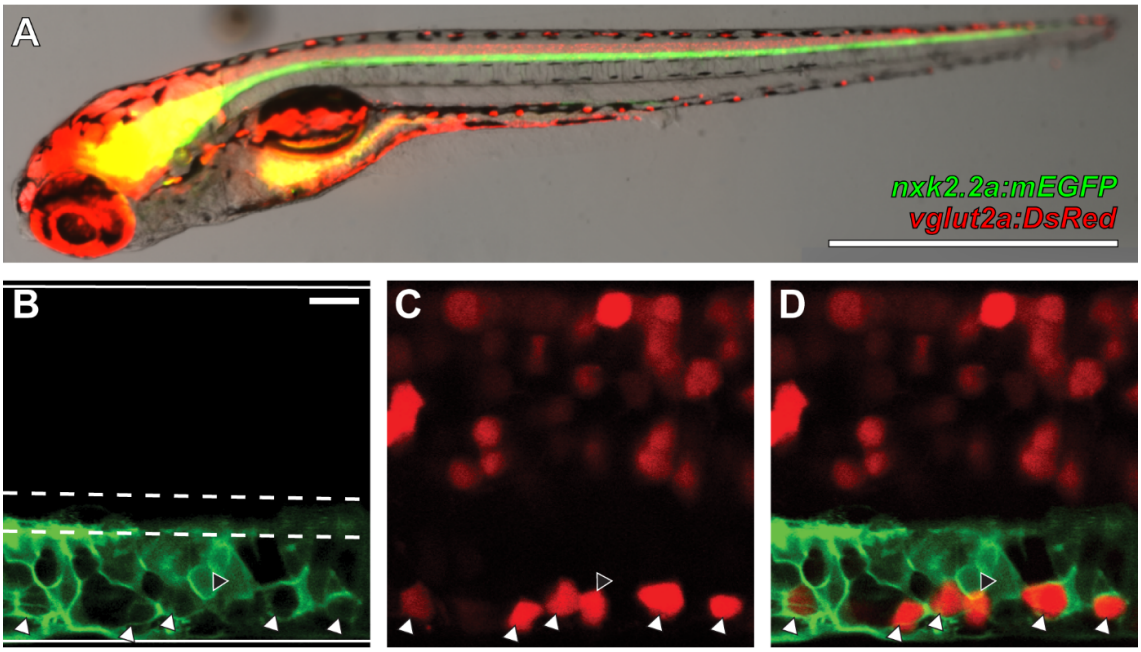

Figure 1. V3-INs are identified by co-localization of *vglut2a:DsRed* and *nkx2.2a:mEGFP* transgene expression in neurons located in the ventromedial spinal cord. (A) Whole-mount *Tg(nkx2.2a:mEGFP)*^{vu17};*Tg(vglut2a:DsRed)*^{nns9} double transgenic zebrafish larva. (B-D) A representative single confocal optical section of the spinal cord exhibiting: (B) *nkx2.2a:mEGFP* expression, (C) *vglut2a:DsRed* expression, and (D) overlayed *nkx2.2a:mEGFP* and *vglut2a:DsRed* expression. The boundaries of the spinal cord and central canal are illustrated by solid and dashed white lines, respectively, in panel B. White triangles indicate neurons that co-express both transgenes and the black triangle indicates the only *vglut2a:DsRed* neuron ventral to the central canal that did not co-express *nkx2.2a:mEGFP* in the field of view. Scale bars: 1 mm in A and 10 μm in B-D.

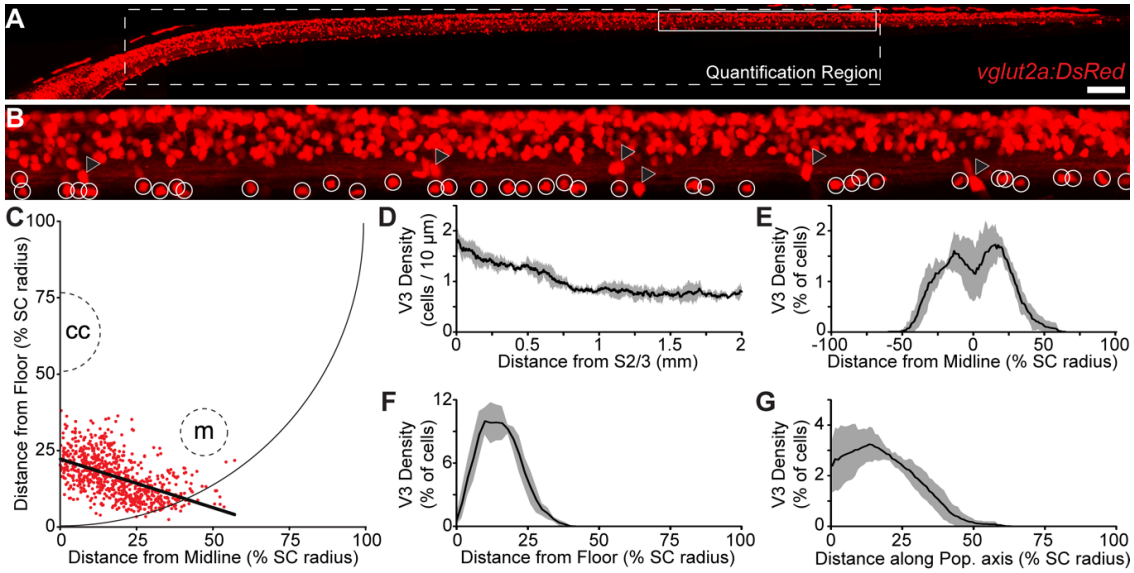

Figure 2. Distribution of V3-IN Cell Bodies in the Spinal Cord. (A) Maximum intensity projection of a confocal stack of the spinal cord of a 5 dpf Tg(*vglut2a:DsRed*)^{nns9} zebrafish larva. The dashed white outline indicates the region of the cord in which cells were quantified. The solid white outline is the region of the image shown at higher magnification in (B). (B) A higher magnification field of view. White circles indicate V3 neurons, black triangles indicate DRG neurons located lateral of the spinal cord. (C) Distribution of location of all quantified V3 neurons (red dots) projected in the coronal plane of the spinal cord. The schematic outline of the spinal cord (solid grey line), as well as the location of the central canal (cc) and Mauthner axon (m), are approximate. The heavy black line indicates the line of best fit that best describes the axis of the V3 neuronal population. (D-G) The windowed moving average of V3 density along the rostrocaudal axis (D; window width: 250 µm), mediolateral axis (E; window width: 15% SC radius), dorsoventral axis (F; window width: 15% SC

932 radius), and along the population axis illustrated in panel C (G; window width:
933 15% SC radius). Black lines are the mean, grey area indicates the standard
934 deviation. SC: spinal cord. Scale bar: 100 μm in A and 19 μm in B.

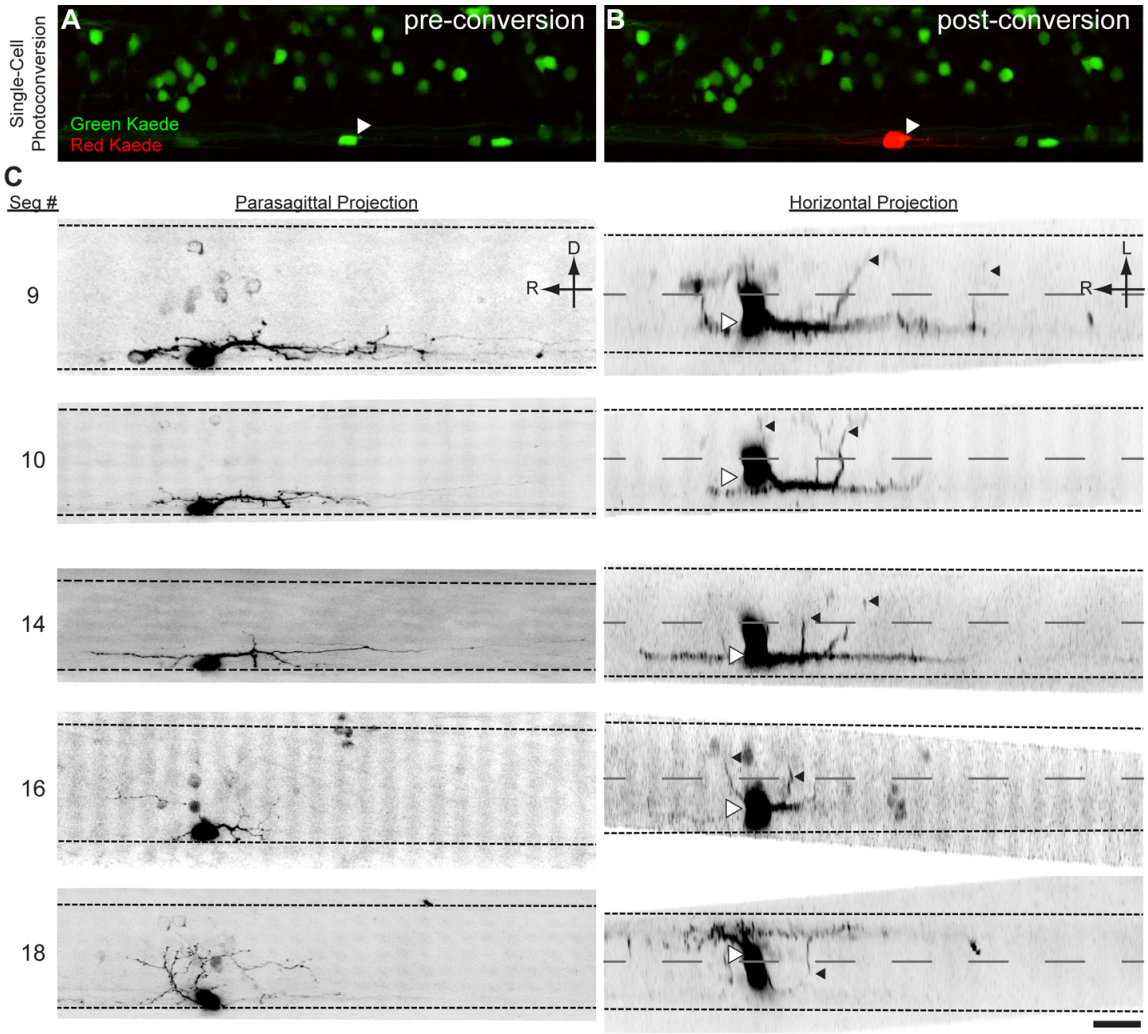

935
936
937 **Figure 3. V3-INs are descending, bilaterally projecting cells.** Kaede was
938 expressed in *vglut2a*-expressing neurons in
939 *Tg(vglut2a:Gal4ff)*^{nns20};*Tg(UAS:Kaede)*^{s1999t} double transgenic larvae (A). A
940 single V3-IN was exposed to UV laser light, converting the Kaede protein from
941 green fluorescence to red (B). (C) Inverted contrast projections of Kaede-red
942 fluorescence in 5 neurons. Each row of images is a neuron shown in a
943 parasagittal projection (left) and horizontal projection (right). On the horizontal
944 projections, the center of the cell body is indicated with white triangles to account
945 for optical bloom and contralateral projections are indicated with black triangles.

946 Lateral projections: Rostral left, dorsal up. Horizontal projections: Rostral left,

947 lateral up. Scale bar: 20 μm.

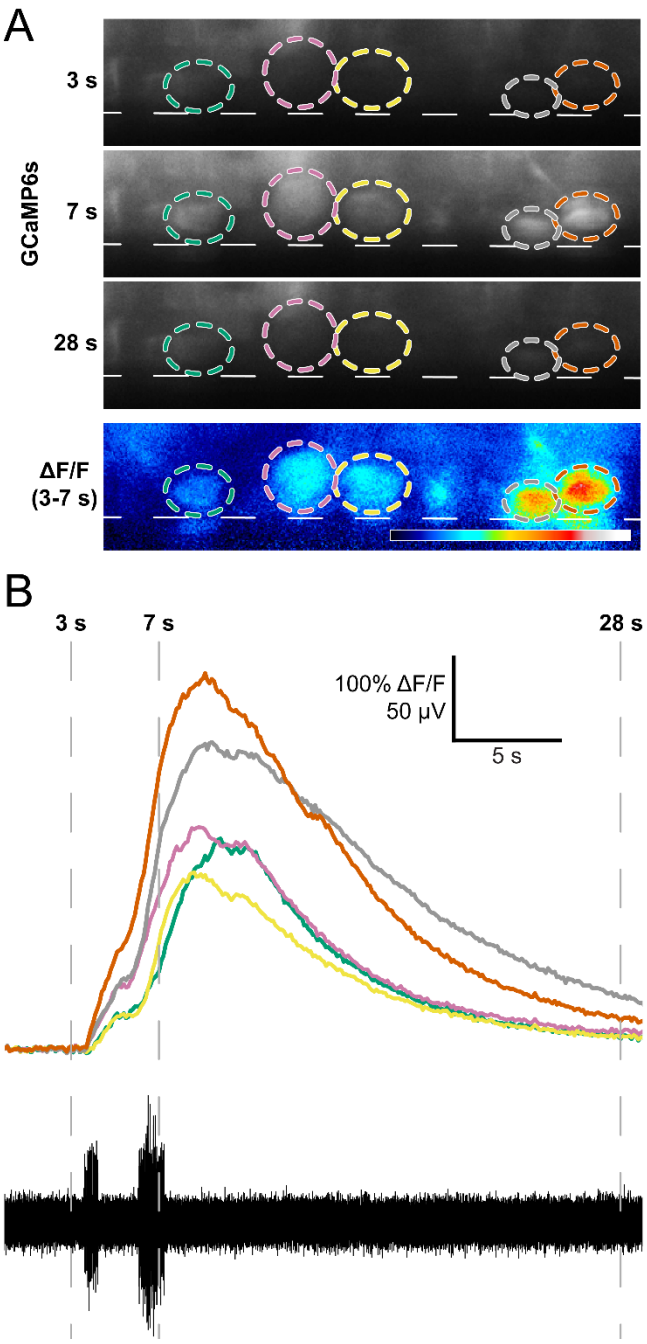

Figure 4. V3-IN activity is temporally correlated to fictive locomotion. (A) Each V3 neuron in the field of view in Tg(*vglut2a:Gal4ff*)^{nns20};Tg(*UAS:GCaMP6s*)^{nk13a} double transgenic larvae was assigned a ROI during spontaneous fictive swimming. Panels in (A) show raw

954 GCaMP6s fluorescence (F) and correspond to numbered time-points in (B).

955 Bottom panel in A shows calculated ΔF/F between 3 and 7 s time-points. Dashed

956 lines represent ventral boundary of the spinal cord. (B) Synchronized recordings

957 of GCaMP6s fluorescence (top) and fictive swimming (bottom) allowed

958 identification of swimming-related neuronal activity.

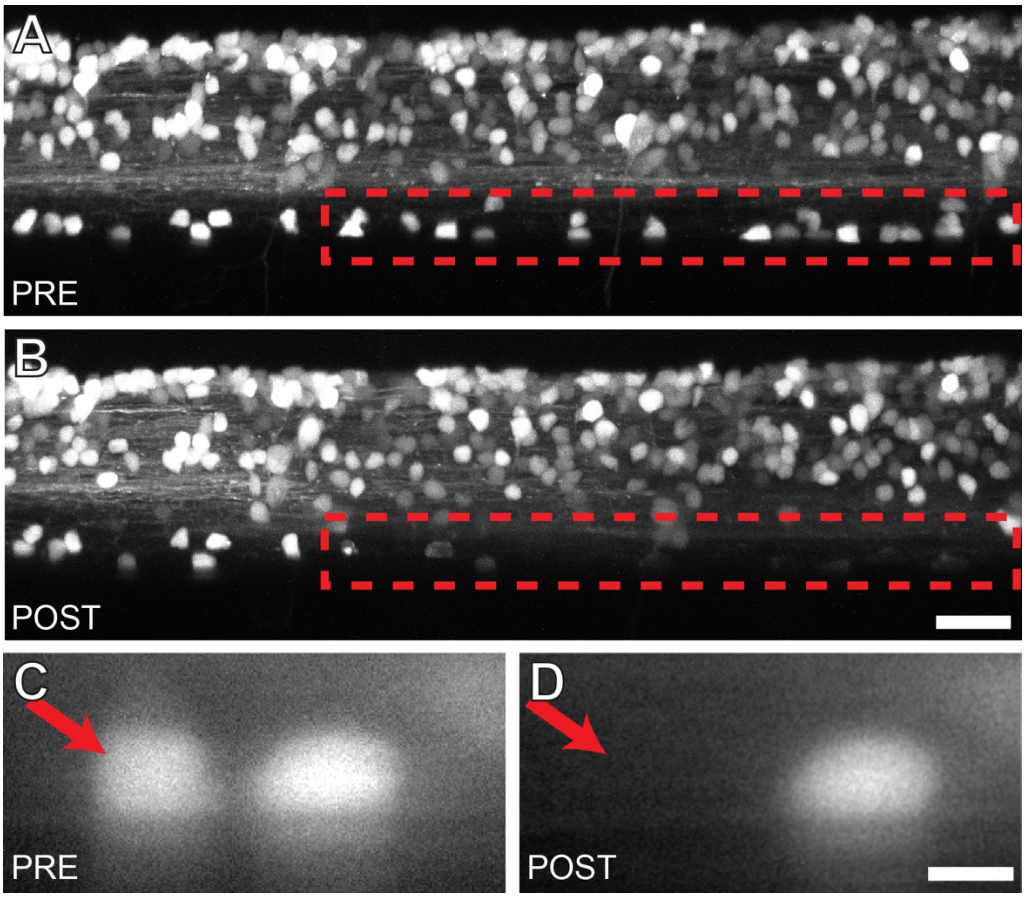

Figure 5. Targeted ablation of V3-INs is both efficient and spatially restricted. (A-B) Confocal stacks of the same Tg(*vglut2a:DsRed*)^{nns9} zebrafish larva before (A) and 12 hours after (B) laser ablation of the V3-INs in the region indicated (red dashed lines). (C-D) A magnified view of two V3-INs before (left) and after (right) a single cell laser ablation. Scale bars: 20 μm in A and B and 5 μm in C and D.

968

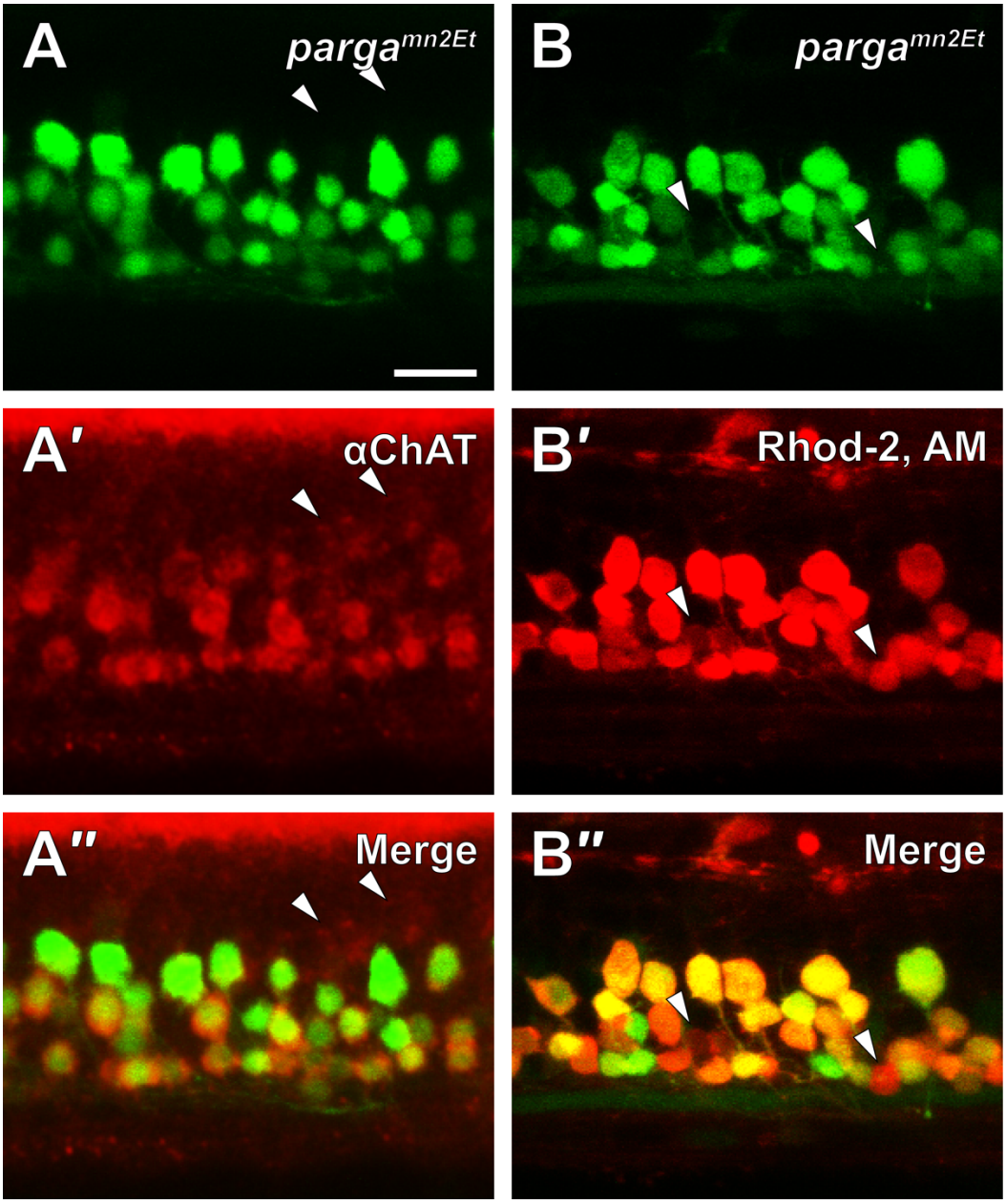

969
970
971 **Figure 6. Spinal neurons loaded with rhodamine-2 AM dye are definitively**

972 **identified as MNs.** (A) The EGFP-expressing *parga*^{mn2Et} enhancer trap line (A,

973 green) was labeled with antibodies to choline acetyl transferase (ChAT; A′, red).

974 Colabeling (A″) of EGFP with ChAT antibodies indicated that EGFP expression in

975 the *parga*^{mn2Et} line is a marker of spinal motor neurons. White arrowheads

976 indicate ChAT-positive cells that do not contain EGFP (non-MNs). (B) Live
977 *parga*^{mn2Et} larvae were anesthetized, skinned, and incubated in rhodamine-2 AM
978 dye (Rhod-2, AM). EGFP expression (B, green) and Rhod-2, AM labeling (B′,
979 red), showed that Rhod-2, AM specifically labeled all motor neurons (B″). White
980 arrowheads indicate two Rhod-2, AM-labeled cells that did not contain EGFP.
981 Scale bar: 20 μm.

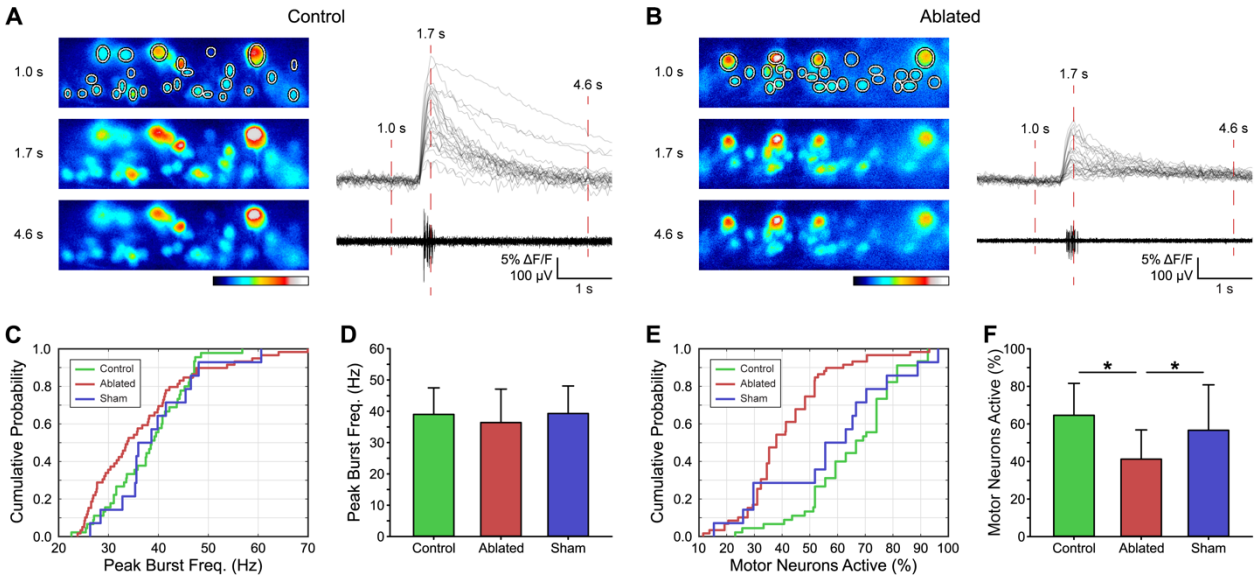

Figure 7. V3-IN laser ablation reduces the proportion of motor neurons that are active during fictive swimming. MNs in *Tg(vglut2a:DsRed)*^{nns9} larvae were loaded with Calcium Green-1 AM dye and assigned ROIs during recording. Synchronous MN fluorescence and fictive swimming recordings were compared between Control, V3-IN Ablated, and Sham ablated preparations. (A and B) Raw Calcium Green-1 AM fluorescence panels correspond to numbered time-points in aligned ΔF/F (each gray line represents a MN) and peripheral nerve traces in a Control preparation (A) and a V3-IN Ablated preparation (B). (C-F) Cumulative probability distributions and mean Peak Burst Frequencies (C and D) and percent of MNs active (10% ΔF/F threshold) during fictive swimming episodes (E and F). Asterisks represent significant differences. Error bars represent SD.

		Episode Duration (msec)	Burst Frequency (Hz)	Burst Duration (msec)
Control (*n* = 6 larvae)		720, SD713	25.7, SD3.4	10.4, SD2.8
Ablated (*n* = 6 larvae)		524, SD223	28.3, SD1.9	11.8, SD2.2
Sham (*n* = 6 larvae)		878, SD642	28.2, SD3.8	11.4, SD2.7
ANOVA	**F**	0.58	1.30	0.42
	p	0.57	0.30	0.67

Table 1. Measures of the episodic and burst properties from peripheral nerve recordings during fictive locomotion in zebrafish larvae. All values presented as mean, standard deviation.